Hindawi
Shock and Vibration
Volume 2018, Article ID 1074340, 15 pages
https://doi.org/10.1155/2018/1074340

Research Article

Experimental Investigation on the Deformation and Fracture of Steel Square Tubes under Double-Explosion Loadings

Chong Ji,[1] **Yang Yu**,[1] **You Zhou**,[2] **Fuyin Gao**,[1] **Xingbo Xie**,[1] **and Jianyu Wu**[1]

[1]*College of Field Engineering, Army Engineering University of PLA, Nanjing 210007, China*
[2]*Northwest Institute of Nuclear Technology, Xi'an 710024, Shanxi, China*

Correspondence should be addressed to Fuyin Gao; 472564948@qq.com

Received 28 May 2018; Revised 26 August 2018; Accepted 29 August 2018; Published 1 November 2018

Academic Editor: Marco Gherlone

The experimental investigations on the square tubes with various stand-off distances and wall thickness were helpful to understand the dynamic response of metal shell under single and double explosion. Therefore, the effect of stand-off distance, wall thickness, and amounts of explosion on the deformation and damage of the square tubes and the regular pattern of the fracture development was analyzed by dimensions of local plastic deformation, volume of the depression area, and crack type. The result reveals that the deformation and fracture mode of steel square tubes gradually transform from local deformation to rupture with the decrease of wall thickness and stand-off distance. Besides, the failure degrees of square tubes under a double explosion were relatively higher than those of square tubes under a single explosion. In addition, the experiment indicates that the side corners of the square tube are very vulnerable, and they are damaged easily by the stress concentration and shear effect. The conclusion provides an important scientific basis for the structural design of square-tube structures and calculation of engineering protection.

1. Introduction

With the frequent occurrence of worldwide terrorist explosions and industrial explosions, research on the antiexplosion capability of engineering structures is attracting increasing attention from international experts. Metal thin-walled hollow members (tubes) have high stiffness excellent energy absorption characteristics, are light weight and easy to process, and are widely used in ocean platforms, gas and petroleum pipelines, construction structures, aerospace industry, and other military or civilian fields. Engineering structures are often damaged by a single or continuous explosion, which means that the structure of a metal thin-walled hollow member may be in danger of multiple explosions. As one of the important forms of thin-walled hollow structures, a square tube will produce local or global plastic deformation or rupture when subjected to an explosion impact load, resulting in the structure losing its original function. In this condition, a more serious damage may occur if it is subjected to explosion impact again. Therefore, the study of the dynamic response mechanism of the square-tube structure under multiple explosion loads is of great engineering application value for predicting the deformation characteristics of the structure and improving its antiexplosion capability.

In recent years, numerous studies on the dynamic response of thin-walled structures such as cylindrical shells subjected to explosion and impact loading have been conducted. Yuen et al. [1] used a series of tests and numerical analysis to obtain the dynamic response of a cylindrical tube under lateral blast load detonated at very close proximity. The experimental results indicated that for a constant stand-off distance, the permanent midpoint deflection increased as the mass of the explosive increased. Larger load diameters appear to cause more damage for the same charge mass. Gao et al. [2] studied the damage of the water-filled cylindrical shell subjected to explosion impact through experiments and numerical simulations. The results show that the existence of water provides a "foundation" pressure for deformation resistance. Song et al. [3] built a mathematical model to analyse the deflection and the deformation angle of the steel circular tubes subjected to lateral blast loads. The calculation results agree well with experiment observations when the

deformation is relatively small. Clubley [4] investigated the influence of long-duration blast loads on the structural response of aluminium cylindrical shell structures. Preliminary modelling predicted a global sway and localised plate buckling, and subsequent experimental testing showed a crushing failure of the shell before any translational movement occurred. Kim et al. [5] investigated energy absorption capability and bending collapse behaviour of an aluminium (Al)/carbon fiber reinforced plastic (CFRP) short square hollow section (SHS) beam under transverse quasistatic loading. Abedi et al. [6] found the pipe displacement and peak particle velocity under a blast wave equivalent dynamic load by establishing a mathematical model. Wu et al. [7] conducted experimental and numerical studies on the dynamic response of metal cylindrical shells under the combined effects of fragments and shock waves and obtained three failure modes. The effects of preformed holes, hole-spacing, and TNT charge at a certain stand-off distance on the deformation/failure of a cylindrical shell were analyzed. Rajabiehfard et al. [8] investigated axisymmetric circular cylindrical shells subjected to axial impact, and two types of loading were analyzed. Rushton et al. [9] carried out an internal charge explosion test for a seamless steel tube with diameter of 324 mm and wall thickness of 9.5 mm. Because of the small amount of explosive used (0.8 kg of PE4 explosive), only the bulge phenomenon of the tube wall was observed. With respect to the square tube, Wegener and Martin [10] investigated the permanent deformation of a simply supported thin-walled square tube under the explosive load of a flake explosive. Bambach [11, 12] tested the local and global deformation of an aluminium alloy square tube subjected to the impact load of an explosion and obtained an empirical formula for calculating its deformation according to the experimental results. Jama et al. [13, 14] theoretically and experimentally studied the dynamic responses of three different sizes of square tubes under uniformly distributed explosion loads and used numerical simulation to gain an insight into the temporal distribution of the global and local deformation and the adiabatic temperature rise in the beams as a result of impulsive loading. Karagiozova et al. [15, 16] developed a model of deformation of a metal hollow section beam under a uniform blast loading, in order to reveal the characteristic features of deformation and energy absorption of hollow section beams under such loading. Jones [17] considered the thin-walled square tube as an ideal rigid-plastic structure and conducted experimental and theoretical studies on its plastic deformation under impact loadings.

The above studies mainly focused on the single-explosion load of thin-walled shell structures, and few studies have been conducted on the blast resistance characteristics of protective structures under multiple explosion loads. With the increasing awareness of security problems in practical applications, the problem of multiple explosions is receiving growing attention. Zhang et al. [18] reduced the multiple blast loads to a series of pulsed loads that were long enough apart. The experiment shows that under the multiple loads, as the number of loads increases, the damage of structural materials gradually increases, and the bearing capacity of the structure decreases. Kumar et al. [19] studied in detail the influence of stand-off distance, explosive amount, strain rate, and provision of stiffeners on the dynamic behaviour of semiburied structure under soil-structure interaction and multiple explosion conditions. Henchie et al. [20] and Yuen et al. [21] studied the impact tests of five similar uniform blast loads on plates, and the impact, deformation, and material changes of plates under multiple blast loads are analyzed. At the same time, ABAQUS is used to simulate the experiment. The numerical simulation results are compared with the experimental results, and the influence of repeated blast loading on the material properties of the test plate is further analyzed. Zhou et al. [22] obtained five different failure modes by studying the double explosions of metal cylindrical shells under different explosive conditions. The results show that the deformed cylindrical shell subjected to the first explosive shock absorbs more energy than the unstructured shell under a given explosive load.

In the above studies, where the scholars mainly focus on the dynamic response of engineering structures under a single explosion and its calculation method, the failure modes and dynamic responses of engineering structures under multiple explosions are rarely studied. Owing to the special structure of the square tube, there are still no published studies on the deformation and damage of steel square tubes subjected to multiple explosions. Therefore, it is of great theoretical significance and application value to study the antiexplosion characteristics of structures under multiple explosive loads.

Field experiments were carried out to investigate the influences of initial conditions on the damage effects of the steel square tube on the side of the local explosion load. Square tubes (with wall thicknesses of 3.0, 3.5, and 4.0 mm) were subjected to a single explosion (of 160 g of TNT charge) and a double explosion (where the first explosion is of 100 g of TNT charge and the second explosion is of 160 g of TNT charge) with different stand-off distances. The failure modes, deflection of the centre of the tube, the radial width, axial length, and volume of the depressed area were analyzed. Through a comparison and analysis of the experimental results, the key factors that affect the deformation of the structure and the influence rules were obtained so as to provide a reference for the antiexplosion capability analysis and prediction of deformation failure mode of the square tube.

2. Experimental Research

2.1. Experimental Setup. The square tubes under the single- and double-explosion tests were Q235 steel square tubes with outer diameter of 100 mm × 100 mm; wall thicknesses of 3.0 mm, 3.5 mm, and 4.0 mm; and length of 100 cm. The chemical composition of the specimen is listed in Table 1. The ordinary mechanical properties are listed in Table 2. The experiment uses cylindrical press-fitting 100 g and 160 g TNT charge columns as explosion sources with dimensions of Φ 48 mm × 34 mm and Φ 48 mm × 54 mm.

The charge was vertically installed above the square tube and aligned with a line passing through its centre point. The centre of the upper surface of the column charge was

Table 1: The chemical compositions of steel Q235.

Elements	C (%)	Si (%)	Mn (%)	P (%)	S (%)
Contents	0.15	0.3	0.35	0.045	0.05

Table 2: Mechanical properties.

Elongation ε_f (%)	Elastic modulus E (GPa)	Yield strength σ_s (MPa)	Tensile strength σ_b (MPa)
26	208	239	430

initiated by an electric detonator. The TNT density is 1.63 g/cm^3, and the detonation velocity is 6950 m/s.

Sketches of the double-explosion experiment setup are shown in Figure 1. The PVC tubes were thin and of low strength and thus had little effect on the experimental results. The square tubes were simply supported on a bracket [2, 6–8]. The contact area between the square tube and the bracket was kept small enough to ensure that this contact area had little influence on the experimental results.

In this study, when the square tube is subjected to the explosion load for the first time (that is, the first time under the explosive load of the 100 g TNT charge), it is defined as the first explosion of the double explosion. When the square tube is subjected to explosion loading again (that is, the second time under the explosive load of the 160 g TNT charge), this is defined as the second explosion of the double explosion. The deformed square tubes under the blast load may be subjected to the explosion impact again anywhere. The first and second explosions of the double-explosion tests were set in the same direction and considering the worst conditions. The stand-off distance was defined as the distance between the bottom of the charge and the midpoint of the front zone of the square tube. When the deformed square tube was subjected to the second explosion, the stand-off distance became the distance from the bottom of the charge to the centre of the depression zone. For the purpose of comparison, the stand-off distances in the first and second explosion tests of the double-explosion experiments were the same. Figure 2 describes in detail the stand-off distance of the first and second explosion tests.

2.2. Experimental Results and Discussion. Thirty-six tests were conducted in this study. The experiment numbers were defined as TZ1 to TZ36. Table 3 lists the final test conditions and results, which include the wall thickness a of the square tube, stand-off distance R, charge mass m, deformation parameters, and failure modes for each test. l_x and l_y are the local plastic deformation values of the oval concave in the axial and radius direction, respectively. δ_{local} and δ_{global} represent the vertical distance from the midpoint and the lowest point of the back zone to the highest point of the square tube, respectively (indicated in Figure 3). V is the volume of the depressed area measured by the filling method, and the measurement method is shown in Figure 4(a). The front zone represents the upper half of the square tube facing the explosion, and the back zone represents the lower half of the square tube against the explosion. When partial cracks are generated, the value of d_1 was recorded as "–." The description

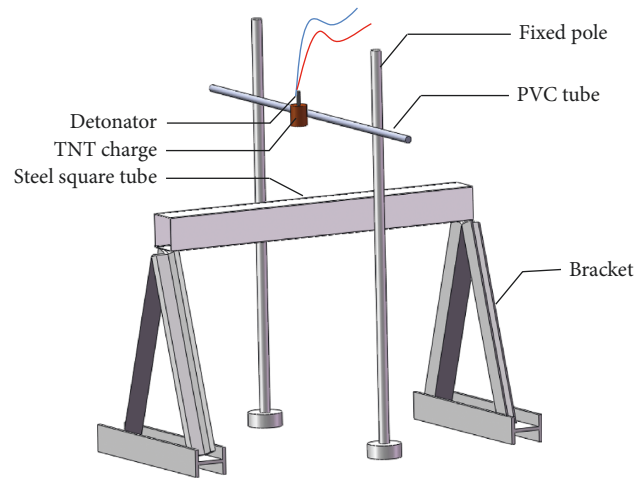

Figure 1: Sketches of experiment setup.

of the plastic hinge is shown in Figure 4(b). The bulge zone is located on the side wall, and the crimp zone is located on the side corners of the square tube. A is the blasting midpoint, J and K are in the axial plastic hinge, and G and H are located at the side corners of the square tube. TZn is the test number. For example, TZn-1 and TZn-2 express the first and second explosion test of the double-explosion test TZn, respectively. The charge mass "100 g + 160 g" represents the two explosion tests of the square tubes subjected to the first and second explosions of the double explosion.

According to the typical beam deformation modes studied by Menkes and Opat [23], Wu et al. [7] studied the damage of cylindrical shells under the combined effect of fragments and shock waves and divided the cylindrical shell deformation into three modes, namely, Mode I, Mode II, and Mode III. Based on the experiment results and previous ones, the deformation of a square tube subjected to double-explosion loadings is divided into four failure modes in this report. Owing to the influence of the machining accuracy and measurement error, when δ_{global} is less than 1.05 times Φ, no global deformation is considered to have occurred in the square tube:

Mode Ia: local plastic deformation at the front zone of square tube, without global deformation ($\delta_{global} \leq 1.05\Phi$)

Mode Ib: local plastic deformation at the front zone of square tube, with small global deformation ($1.05\Phi < \delta_{global} \leq 1.4\Phi$)

Mode II: coupling of local cracking deformation and global deformation, and the crack presents a radial H-type crack

Mode III: coupling of local cracking deformation and global deformation, and the crack presents an axial H-type crack

3. Discussion

3.1. Analysis of Typical Failure Modes. Figure 5 shows the two typical deformation modes of a square tube under double-explosion loads, namely, Mode Ia and Mode Ib. It is

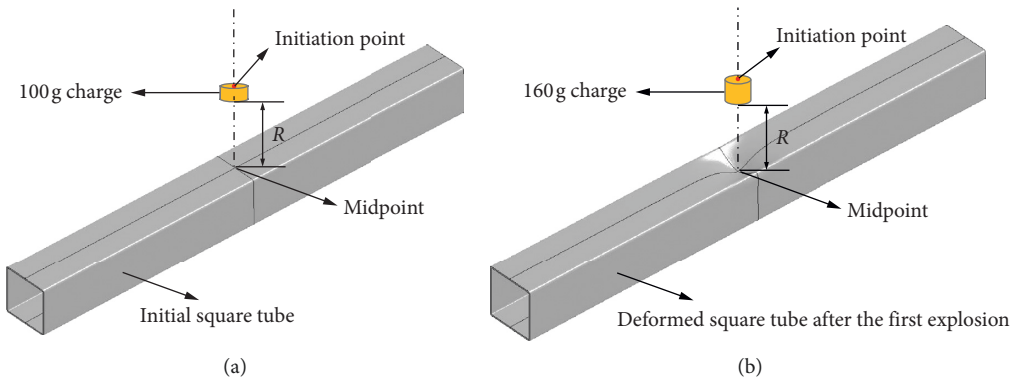

Figure 2: Stand-off distance description of the first and second explosion test. (a) The first explosion of double-explosion test. (b) The second explosion of double-explosion test.

Table 3: Detailed experimental data of the single- and double-explosion tests.

Test no.	Test conditions			Experimental results							
	a (mm)	R (cm)	m (g)	l (mm)	l_x (mm)	l_y (mm)	d (mm)	V (ml)	δ_{local} (mm)	δ_{global} (mm)	Failure mode
TZ1	3.0	24	100 + 160	106.7	357.3	73.3	61.3	196.6	42.2	103.5	Mode Ia
TZ2	3.0	24	160	100.8	308	80.8	71.0	155.8	31.7	102.7	Mode Ia
TZ3	3.0	22	100 + 160	107.5	360.9	73.4	58.7	205	45.8	104.5	Mode Ia
TZ4	3.0	22	160	102.1	322	80.0	70.0	161.1	33.2	103.2	Mode Ia
TZ5	3.0	20	100 + 160	109.5	365.8	69.2	53.0	216.6	53.1	106.1	Mode Ib
TZ6	3.0	20	160	103.1	307	78.7	69.3	171.7	34.2	103.5	Mode Ia
TZ7	3.0	18	100 + 160	115.7	339.5	76.4	–	238.9	108.0	108.0	Mode II
TZ8	3.0	18	160	104.6	314	76.1	64.3	183.7	39.8	104.1	Mode Ia
TZ9	3.0	16	100 + 160	117.8	340	80.3	–	298.7	112.3	112.3	Mode III
TZ10	3.0	16	160	107.2	322	68.6	54	205	50.7	104.7	Mode Ia
TZ11	3.0	12	100 + 160	115.5	305.6	112.9	–	–	141.5	141.5	Mode III
TZ12	3.0	12	160	110.0	327	64.0	44.8	225.3	63.1	107.9	Mode Ib
TZ13	3.5	22	100 + 160	103.2	273	85.1	77.0	106.7	26.5	103.5	Mode Ia
TZ14	3.5	22	160	101.0	264	87.2	82	84.7	20.4	102.4	Mode Ia
TZ15	3.5	20	100 + 160	103.9	288	80.7	74.2	111.8	29.5	103.7	Mode Ia
TZ16	3.5	20	160	101.3	253	84.6	81.3	87.6	21.4	102.7	Mode Ia
TZ17	3.5	18	100 + 160	109.1	292	78	66.6	119.1	37.9	104.5	Mode Ia
TZ18	3.5	18	160	102.5	251	82.4	76.3	106.7	26.7	103	Mode Ia
TZ19	3.5	16	100 + 160	108.0	304	77.1	61.4	166.4	43.5	104.9	Mode Ia
TZ20	3.5	16	160	103.5	253	77.2	75.5	116.3	28.1	103.6	Mode Ia
TZ21	3.5	14	100 + 160	112.3	284	78.8	–	234	102.5	102.5	Mode II
TZ22	3.5	14	160	104.6	256	76.7	69.4	142	34.7	104.1	Mode Ia
TZ23	3.5	12	100 + 160	115.5	268	87.3	–	–	116.9	116.9	Mode II
TZ24	3.5	12	160	105.4	262	76.3	66.2	150.5	39.5	105.7	Mode Ib
TZ25	4.0	20	100 + 160	102.8	269.8	81.9	76.2	96.5	25.8	102	Mode Ia
TZ26	4.0	20	160	100.6	257	86.0	83.6	53	18.5	102.1	Mode Ia
TZ27	4.0	18	100 + 160	105.1	278.3	80.9	72.9	99.1	29.8	102.7	Mode Ia
TZ28	4.0	18	160	102.0	246.1	84.7	79.8	58.6	22.5	102.3	Mode Ia
TZ29	4.0	16	100 + 160	104.7	287.9	78.2	65.9	106.7	37.1	103	Mode Ia
TZ30	4.0	16	160	102.5	265	83.0	76.8	69.9	25.8	102.6	Mode Ia
TZ31	4.0	14	100 + 160	106.1	292.7	77.8	60.7	116.3	43.4	104.1	Mode Ia
TZ32	4.0	14	160	103.2	254	81.0	74.8	84.7	28.4	103.2	Mode Ia
TZ33	4.0	13	100 + 160	107.2	283.7	74.2	–	127.7	105.3	105.3	Mode II
TZ34	4.0	13	160	103.9	256	79.0	71.4	106.7	32.1	103.6	Mode Ia
TZ35	4.0	12	100 + 160	110.2	276.5	74.9	–	150.5	107.8	107.8	Mode II
TZ36	4.0	12	160	104.5	266	78.8	68.7	119.5	35.8	104.5	Mode Ia

recorded as Mode Ia and Mode Ib when the square tube only subject to local plastic deformation at the front zone.

The shock wave and detonation product first act on the blasting midpoint and then gradually expand to the zone near the blasting midpoint, when the stress received at the blasting midpoint exceeds its yield strength. Local plastic deformation occurs when the stress generated at the blasting midpoint by the explosion is greater than the yield strength of the square tube.

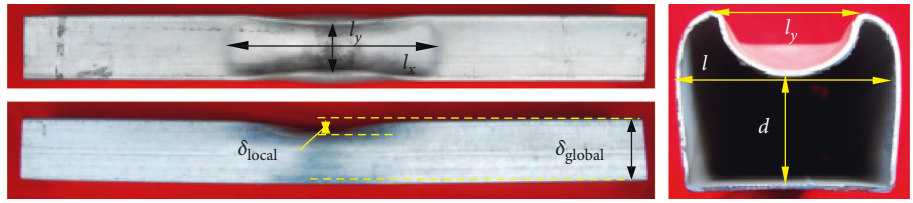

Figure 3: Description of the parameters of the deformation.

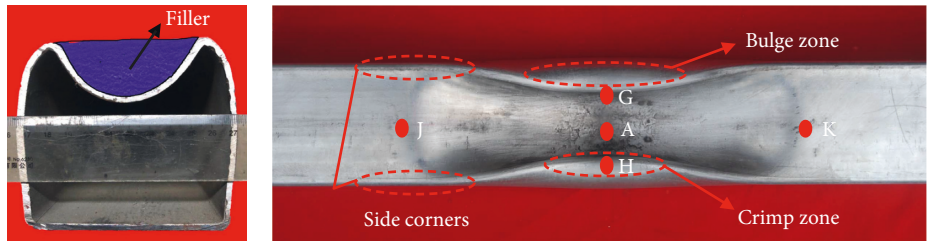

Figure 4: Description of the measurement methods and plastic hinge of square tube deformation. (a) Measurement methods. (b) Plastic hinge.

With further action of the shock wave, the depression zone of the square tube expands to the axial and radial directions, and the depth and area of the depression zone also increased. Owing to the limitation of the cross-sectional shape of the square tube, the axial velocity of the depression zone is higher than that in the radial direction. When the depression zone is developed in the radial direction, the side corners of the square tube are subjected to the pull of the centre of the square. The side corners develop to the centre in the radial direction and the axially inclined deformation develops to both sides, and ultimately an hourglass deformation is formed. When the square tube deformation of Mode Ia occurs, the energy absorbed by the square tube is mainly transformed into the plastic work that produces the local plastic deformation. For Mode Ib, the energy absorbed by the square tube is also converted into the energy of the global deformation.

Figure 6 shows the typical deformation of the square tube under double-explosion loadings in Mode II. With the decrease of the stand-off distance or wall thickness, the deformation and degree of damage of the square tube increase gradually. When the stress received at the midpoint exceeds the ultimate rupture stress and the square tube begins to crack and fail, then plastic deformation and crack growth occur simultaneously. From Figure 6(a), we can see that the crack of critical rupture of the tube develops along the axial direction from the midpoint under double-explosion loadings. With the decrease in stand-off distance, the explosive load acting on the square tube increases. The energy of the explosive load has residual energy in addition to a similar axial crack, as depicted in Figure 6(a), and the crack that develops in axial direction is converted into radial direction and finally forms an H-type crack with radial cracking in Figure 6(b). In Mode II, the energy generated by the explosion on the square tube first causes local plastic deformation and small global deformation of the steel tube, and a part of the energy causes the square tube to crack when the stress exceeds the yield strength of the square tube.

Figure 7 shows the failure mode of Mode III under the double-explosive loadings. As we can see from Figure 7(b), the front zone of the square tube is completely ruptured in the centre of the blasting surface under the action of the high explosive load. The resulting high-speed fragments hit the back zone to produce a certain amount of bulge, and the fragments accumulate in the bulge. The front zone has a broken gap with a size of 141.7 mm × 91.7 mm and the square tube has a larger global deformation. The side corners of the square tube facing the blasting surface have longer cracks in the axial direction, and the fragments generated at the same time impact the back zone with high speed, resulting in a long crack in the axial direction of the side corners of the back zone. Finally, the axial H-type cracking appears. Besides, the explosive load acts on the tube when the side corners in addition to the explosive load have a downward force, while the side walls of the square tube generate an upward support force on the side corners, that is, the side corners are subjected to a pair of strong shear forces. Therefore, the side corners are easily broken by shear failure, and this rupture is easy to develop rapidly along the axial direction of the side corners. Figures 7(a) and 7(b) confirm this statement; there is no obvious thinning on the side corners, and the rupture is neat and in a 45° angle, which is the typical characteristic of a shear failure.

As a contrast, Mode III presents a completely different crack development path from that in Mode II, and the crack of Mode II is more localised on the front zone. Owing to the influence of the side corners of the square tube, the cracks of Mode III are along the side corners, and there are radial cracks and bulging on the side walls of the tube. The side corners of the tube are the junction of the blasting surface and the side walls, and thus, it is easy to produce stress concentration there. In addition, the side corners of the front zone will be subjected to the larger tension of the blasting midpoint and to the intermediate movement under the

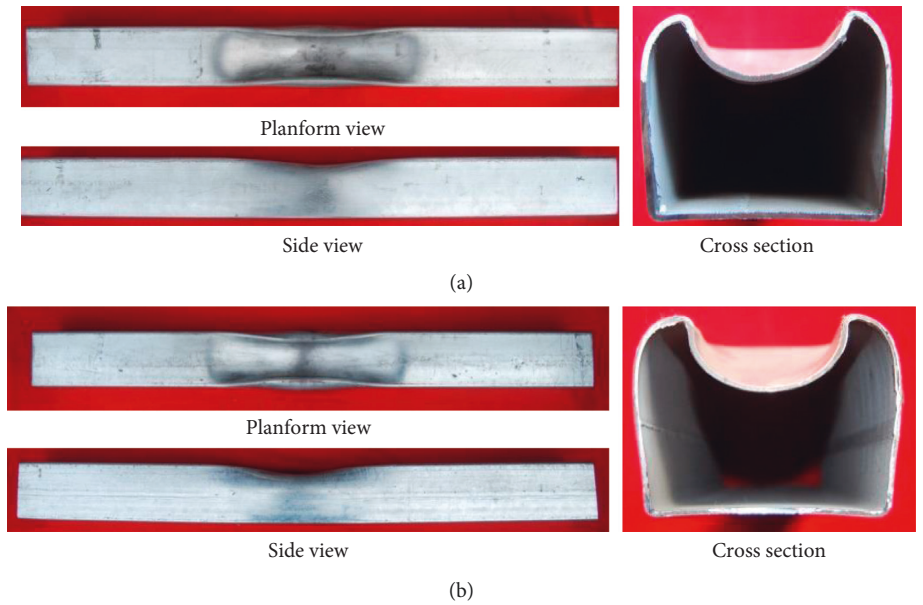

Figure 5: Typical failure modes of cylindrical shell in Mode Ia and Mode Ib. (a) Mode Ia: local plastic deformation without global deformation (a = 3.0 mm, R = 24 cm, m = 100 g + 160 g, TZ1). (b) Mode Ib: local plastic deformation with small global deformation (a = 3.0 mm, R = 20 cm, m = 100 g + 160 g, TZ5).

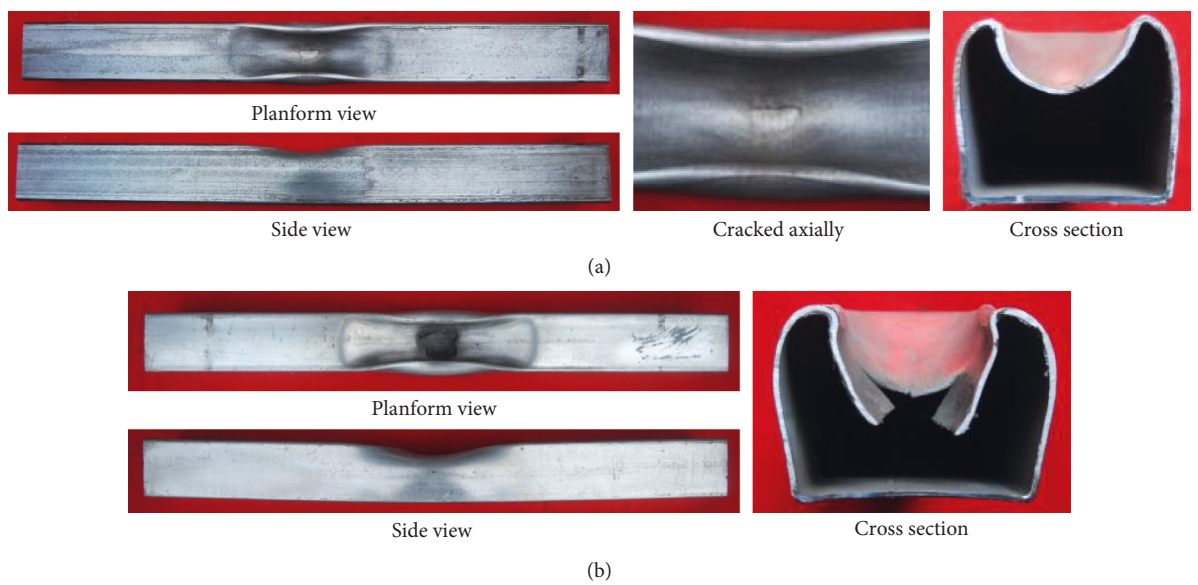

Figure 6: Typical failure modes of square tube in Mode II. (a) The square tube is just cracking (a = 4.0 mm, R = 13 cm, m = 100 g + 160 g, TZ33). (b) The crack presents a radial H-type crack (a = 3.0 mm, R = 18 cm, m = 100 g + 160 g, TZ7).

action of the explosive load. Besides, the side corners of the tube can also be crimped during the movement process, resulting in a more severe stress concentration.

3.2. Deformation and Damage Comparison of Square Tubes under Single and Double Explosion. The predamage on the surface of square tube will decrease the strength of the tube and cause stress concentration thereby making the tube vulnerable to impact load. The final deformation and fracture of the thin-walled square tube is closely related to the interaction between these two factors. The effects of single- and double-explosion loads on the dynamic response of thin-walled cylindrical shells are discussed below.

Figure 8 shows the deformation and fracture comparison of square tubes with different wall thicknesses under a single and double explosion. It can be seen that the deformation and damage of the square tube under the action of the double explosion was more severe than that under the single explosion. Obviously, the deformation modes of the square tubes under a single-explosion load are Mode Ia and Mode Ib, while the deformation modes under double-explosion

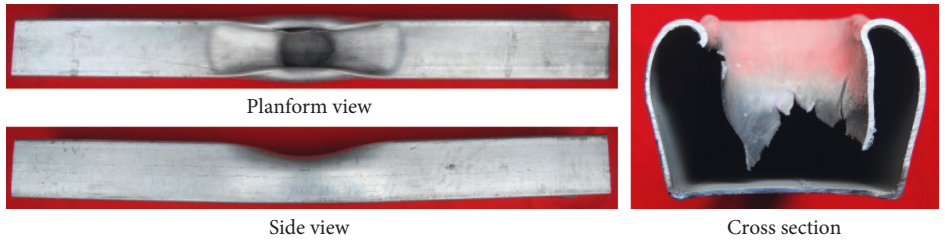

(a)

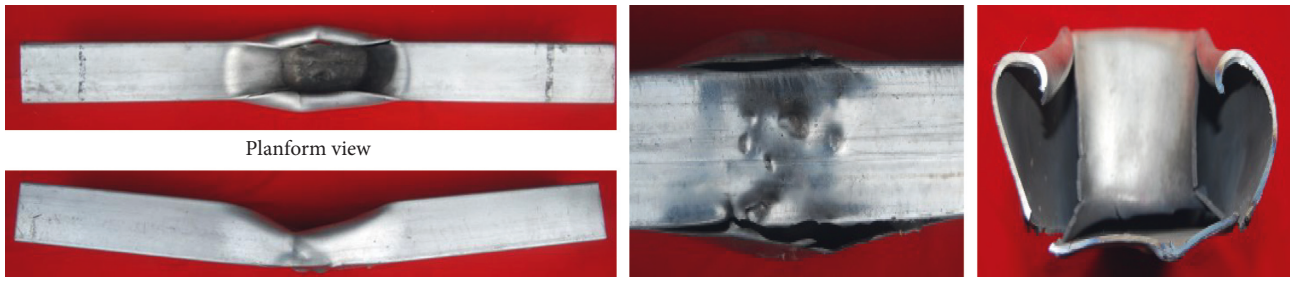

(b)

FIGURE 7: Typical failure modes of square tube in Mode III. (a) The crack presents an axial H-type crack (back without penetration) (a = 3.0 mm, R = 16 cm, m = 100 g + 160 g, TZ9). (b) The crack presents an axial H-type crack (back penetration) (a = 3.0 mm, R = 12 cm, m = 100 g + 160 g, TZ11).

loadings may be Mode Ia, Mode Ib, Mode II, and Mode III. From the comparison between Figures 8(a) and 8(c), it can be seen that the deformation and damage of the square tubes under the single and double explosion are more obvious when the stand-off distance is smaller or the wall thickness is thinner. In Figure 8(a), under the condition of a = 4.0 mm and R = 20 cm, the local plastic deformation of the blasting point of the tube under the single explosion is 18.5 mm, while the deformation under the double explosion is 25.8 mm, and both of them are Mode Ia. However, in Figure 8(c), under the condition of a = 3.0 mm and R = 12 cm, the local plastic deformation of the blasting point of the tube under the single explosion is 63.1 mm, while the deformation under the double explosion is 141.5 mm. The deformation mode of the former is Mode Ib and that of the latter is Mode III, and the difference between the deformation parameters and the deformation model is very large.

Figure 9 illustrates the failure grade comparison of square tubes under single explosion and double explosions. The failure grades from 1 to 4 corresponded to the failure modes from Mode Ia to Mode III. A high-failure grade value resulted in severe damage of the square tubes. Therefore, the failure grades of square tubes under double explosions were relatively higher than those of square tubes under single explosion. When the stand-off distance or the thickness was small, the failure grade difference was remarkably obvious.

In order to study quantitatively the relationship between the single-explosion and double-explosion effects of V in the depression area, the gain coefficient w of the depression area V is introduced. Among them, the gain coefficient w is defined as

$$w = \frac{V_d}{V_s}, \tag{1}$$

where V_d is the volume in the depression area with double explosions and V_s is the volume in the depression area with a single explosion. According to the definition in this study and the experimental data in Table 3, the calculation results of the single-explosion and the double-explosion intervals are compared with that shown in Figure 10.

As shown in Figure 10, the gain coefficient w between the single explosion and the double explosion is 1.26–1.5. The energy absorbed by the square tube under the double explosion is much larger than that absorbed under the single explosion, resulting in greater deformation damage.

When the square tube is subjected to the first explosion of the double explosion, there is a local depression in the front zone of the blasting surface and the square tube is subjected to local plastic deformation and small global deformation. When the tube is subjected to the second explosion of the double explosion, it easily leads to stress concentration in the deformed depression zone, resulting in the decrease of the bearing capacity of the square tube and the reduction of its antiexplosion capability. In addition, owing to the tensile plastic deformation of the front zone caused by the first explosion, the wall thickness of the front zone thins and the ultimate tensile strength is reduced. Therefore, under the same explosion loading, the degree of deformation and damage under a double explosion was evidently higher than that under a single explosion, namely, the predamaged square tube is more susceptible to damage than an undamaged tube when it undergoes the explosion loading again.

3.3. Influence of the Stand-Off Distance on the Dynamic Response of the Square Tubes Subjected to Double Explosion. Previous work on free field explosions indicates that the peak overpressure of the blast increases with decreasing stand-off

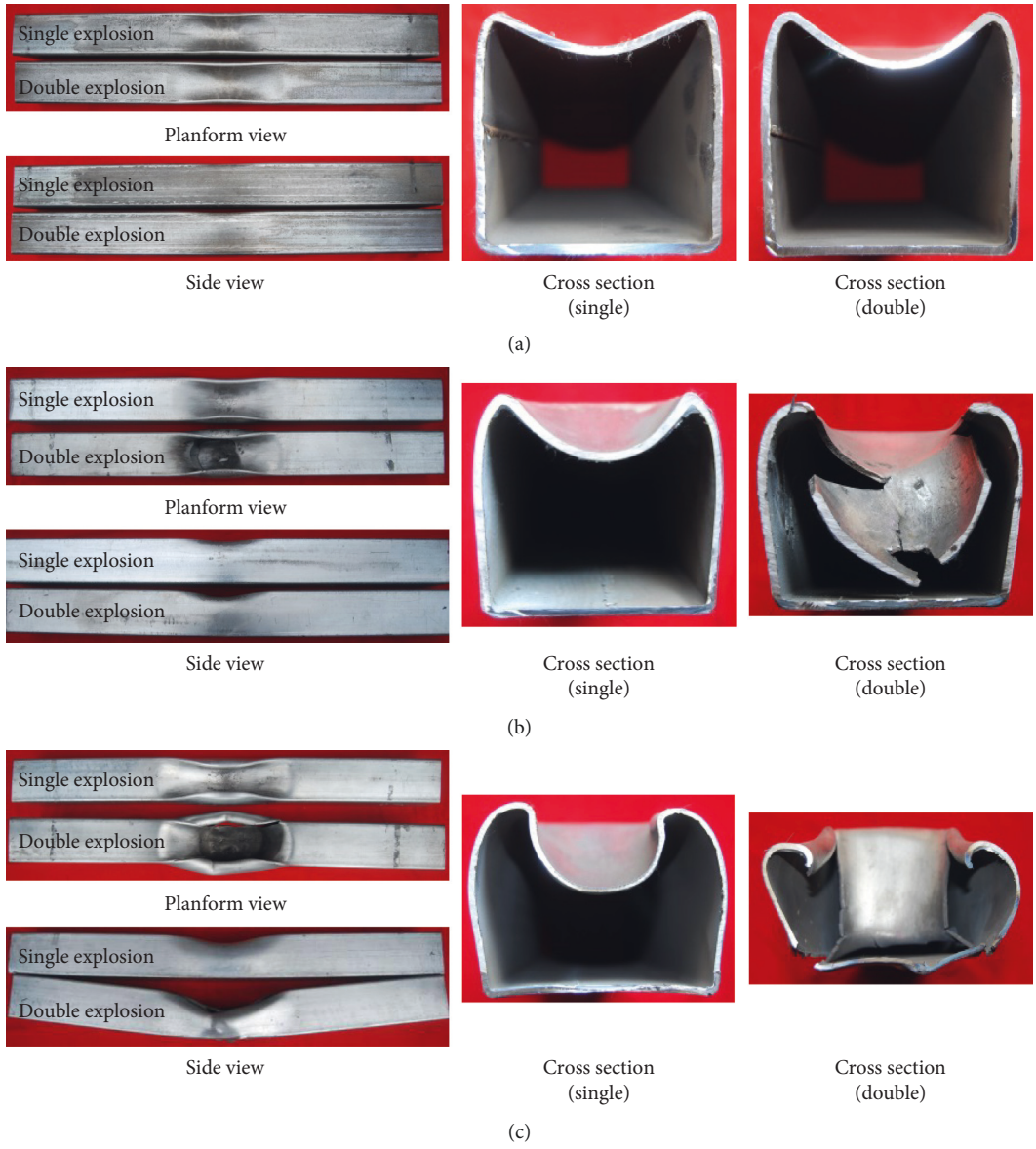

FIGURE 8: The deformation and damage comparison of square tubes subjected to single and double explosions. (a) $a = 4.0$ mm, $R = 20$ cm. (b) $a = 3.5$ mm, $R = 14$ cm. (c) $a = 3.0$ mm, $R = 12$ cm.

distance [21, 22, 24, 25]. Figures 11–14 depict various deformations of square tubes with wall thicknesses of 3.0, 3.5, and 4.0 mm under double-explosion loadings. The charge stand-off distances in these experiments were set to 24, 22, 20, 18, 16, 14, 13, and 12 cm. The results indicate that the degree of plastic deformation zone and crack length of square tubes become gradually more severe as the stand-off distance decreases.

In Figure 12, the stand-off distances in these six double-explosion experiments are 24, 22, 20, 18, 16, and 12 cm. When the stand-off distances are 24, 22, and 20 cm, the deformation mode of the square tube belongs to either Mode Ia or Mode Ib, and the dimensions of their local plastic deformation ($l_x \times l_y$) are 357.3 mm × 73.3 mm, 360.9 mm × 73.1 mm, and 365.8 mm × 69.2 mm, respectively. Local plastic deformation occurred on the tube due to the blasting centre is far from the front zone of the steel tube. This mechanism belongs to deformation Mode Ia and Mode Ib.

When the stand-off distance is decreased from 20 cm to 18 cm, the deformation mode of the square tube is transformed from Mode Ib to Mode II, and their local plastic deformation dimensions ($l_x \times l_y$) are 365.8 mm × 69.2 mm and 339.5 mm × 76.4 mm, respectively. The impact loads in the front zone of the tube increased as the stand-off distance decreased, which causes the tube to crack and a certain global deformation. However, the plastic deformation dimension decreases, even though the stand-off distance decreases. This is because the energy of square tube will not only cause the local plastic deformation of the tube, but also the most energy will be transformed into the fracture energy.

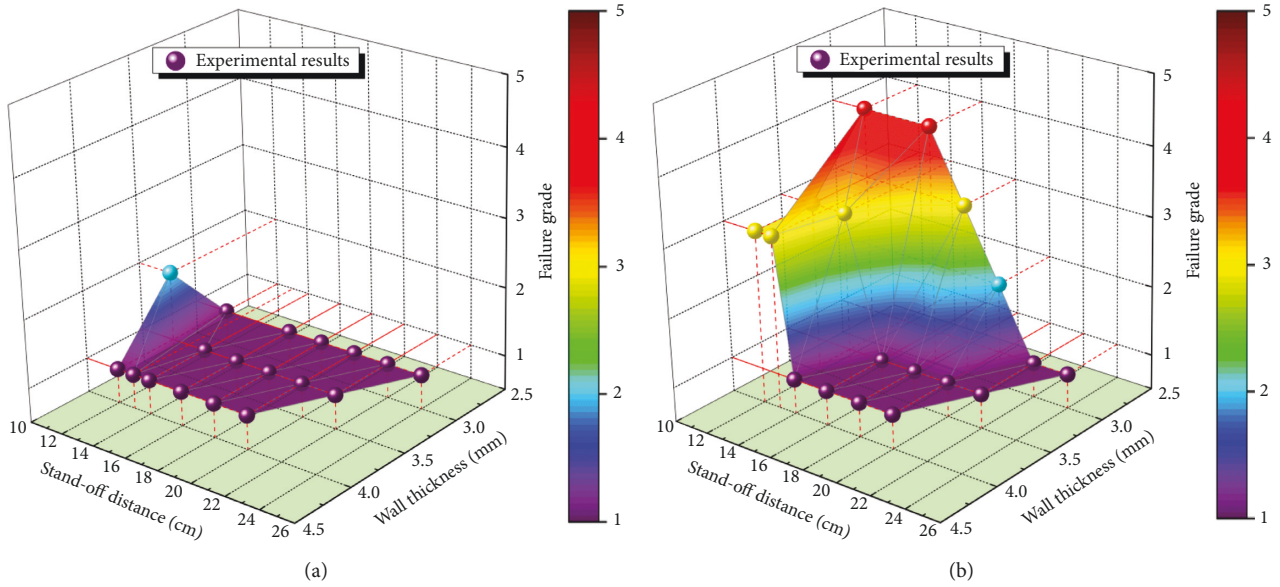

Figure 9: The failure grade of square tubes under single and double explosions. (a) Failure grade under single explosion. (b) Failure grade under double explosion.

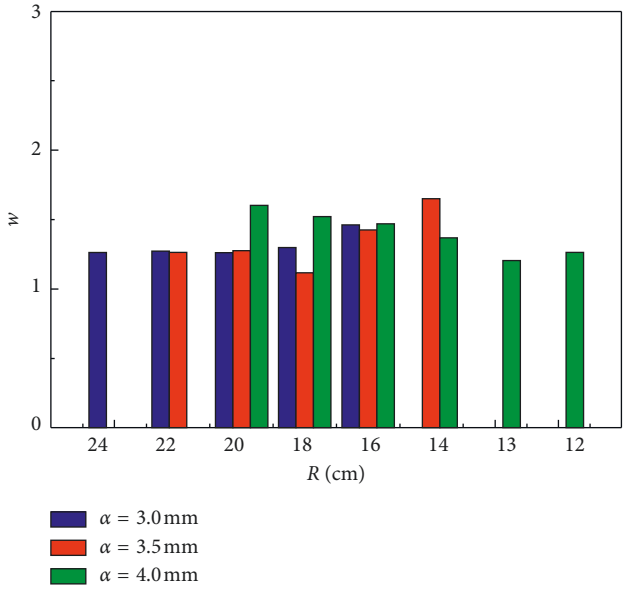

Figure 10: The volume relation between the single and double explosions.

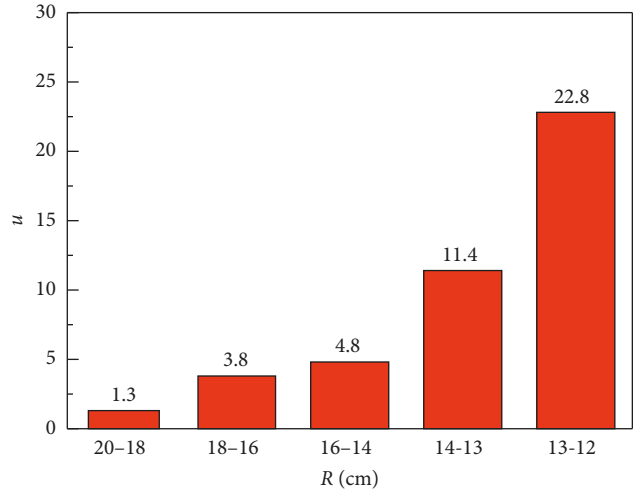

Figure 11: Depression area volume changes with the stand-off distance.

When the stand-off distance is decreased from 18 cm to 16 cm, the deformation mode of the square tube is transformed from Mode II to Mode III, and the axial deformation value l_x of the square tube is almost invariable, and the radial deformation value l_y of the square tube is obviously increased. G and H move towards the blasting midpoint of A under the pull effect; besides, they will move downward under the action of the explosive load and also have a bulging motion on the side walls. Therefore, the square tube at the G and H points appears crimped, and the bulge on the side walls is enlarged. When the stand-off distance continues to decrease from 16 cm to 12 cm and the failure mode of the square tube transforms from Mode II to Mode III, the rupture damage and the plastic deformation zone increase; correspondingly, the axial plastic deformation value l_x decreases from 340 mm to 304.6 mm, and the radial plastic deformation value l_y increases from 80.3 mm to 112.9 mm, respectively. This result indicates that as the stand-off distance is further reduced, the shock wave on the square tube becomes further strengthened and the blast plastic deformation zone becomes enlarged once again.

In order to quantitatively study the damage and failure effect of the stand-off distance R and the influence of V in the depression area, taking the wall thickness a as 4.0 mm, for example, the gain coefficient u of the depression area V with the stand-off distance R is introduced. The gain coefficient u is defined as

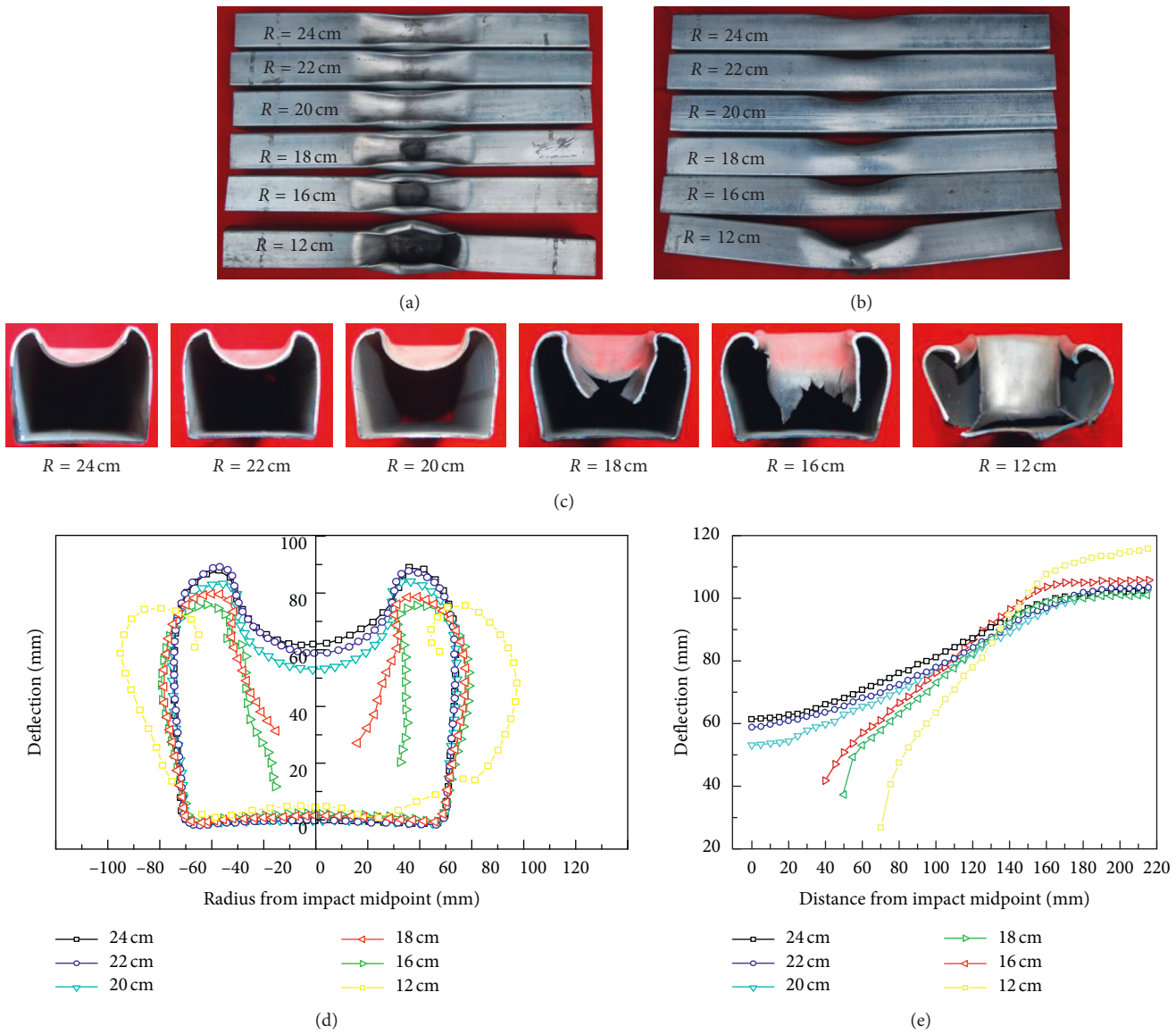

Figure 12: Damage of square tubes with a thickness of 3.0 mm at different stand-off distances. (a) Planform view. (b) Side view. (c) Cross section. (d) Deformation curve on cross section. (e) Deflection in axial direction.

$$u = \frac{V_2 - V_1}{R_2 - R_1}, \tag{2}$$

where the stand-off distances R_1 are 12, 13, 14, 16, and 18 cm, respectively, and V_1 is the volume of the depression area corresponding to the stand-off distance R_1. The stand-off distances R_2 are 13, 14, 16, 18, and 20 cm respectively, and V_2 is the volume of the depression area corresponding to the stand-off distance R_2. According to the definition in this study and the experimental data in Table 3, the calculation results of the stand-off distance in a 12–20 cm interval are compared with those shown in Figure 11.

As shown in Figure 11, the volume growth rate of the depressed area increases when the stand-off distance R is reduced from 20 cm to 12 cm (u from 1.3 to 22.8). It can be seen that with the decrease in stand-off distance, the damage of the explosion load to the square tube is greater and the volume of the depression increases.

Similar laws are also found in Figures 13 and 14. Through the above law, it can be seen that the degree of deformation and damage of the square tubes become gradually more severe as the stand-off distance decreases. A part of the energy absorbed by the square tube is converted to rupture damage energy and global deformation of the tube. Figures 12(d) and 12(e) show the deformation of the square tube more clearly by the description of the cross section and axial deflection. When the stand-off distance decreases from 24 cm to 18 cm, the global deformation value, δ_{global}, increases by 4.5 mm, namely, from 103.5 mm to 108 mm, compared with the

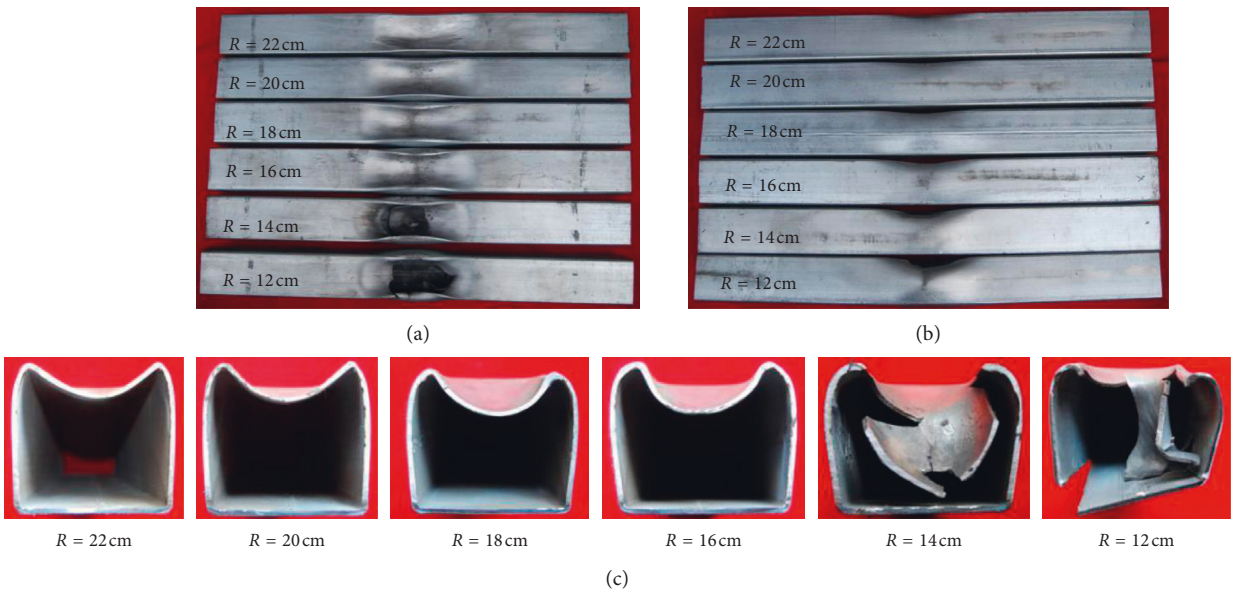

Figure 13: Damage of square tubes with a thickness of 3.5 mm at different stand-off distances. (a) Planform view. (b) Side view. (c) Cross section.

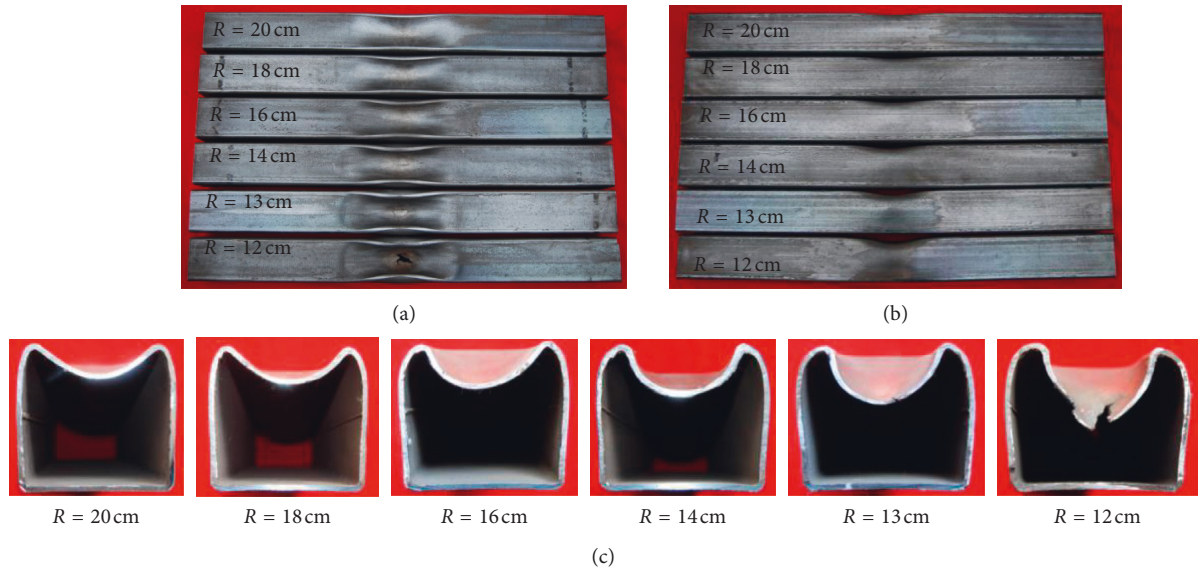

Figure 14: Damage of square tubes with a thickness of 4.0 mm at different stand-off distances. (a) Planform view. (b) Side view. (c) Cross section.

case where the stand-off distance is reduced from 18 cm to 12 cm, in which it increases by 33.1 mm, namely, from 108 mm to 141.1 mm. This result demonstrates that the deformation and damage of the steel tube is quite large or even the fracture deformation occurs, although the charge distance decreases the same size. This difference is attributed to the fact that the shock wave pressure is exponentially attenuated as the propagation distance increases and the attenuation amplitude is larger in the area near the explosion for the same propagation distance. Besides, the explosion load on the blasting surface of the square tube is the common effect of the explosion products and the shock wave in the near distance from the blasting centre, while the explosion load is mainly due to the effect of the shock wave at the larger stand-off distance.

3.4. Influence of Wall Thickness on the Dynamic Response of Square Tubes Subjected to Double Explosion. Figures 15–17 depict various deformations of square tubes with stand-off distance of 18, 16, and 12 cm under double-explosion loadings. Three sizes of wall thickness were selected as 1, 2, and 3 in this test. The results indicate that the degree of plastic deformation zone and crack length of square tubes

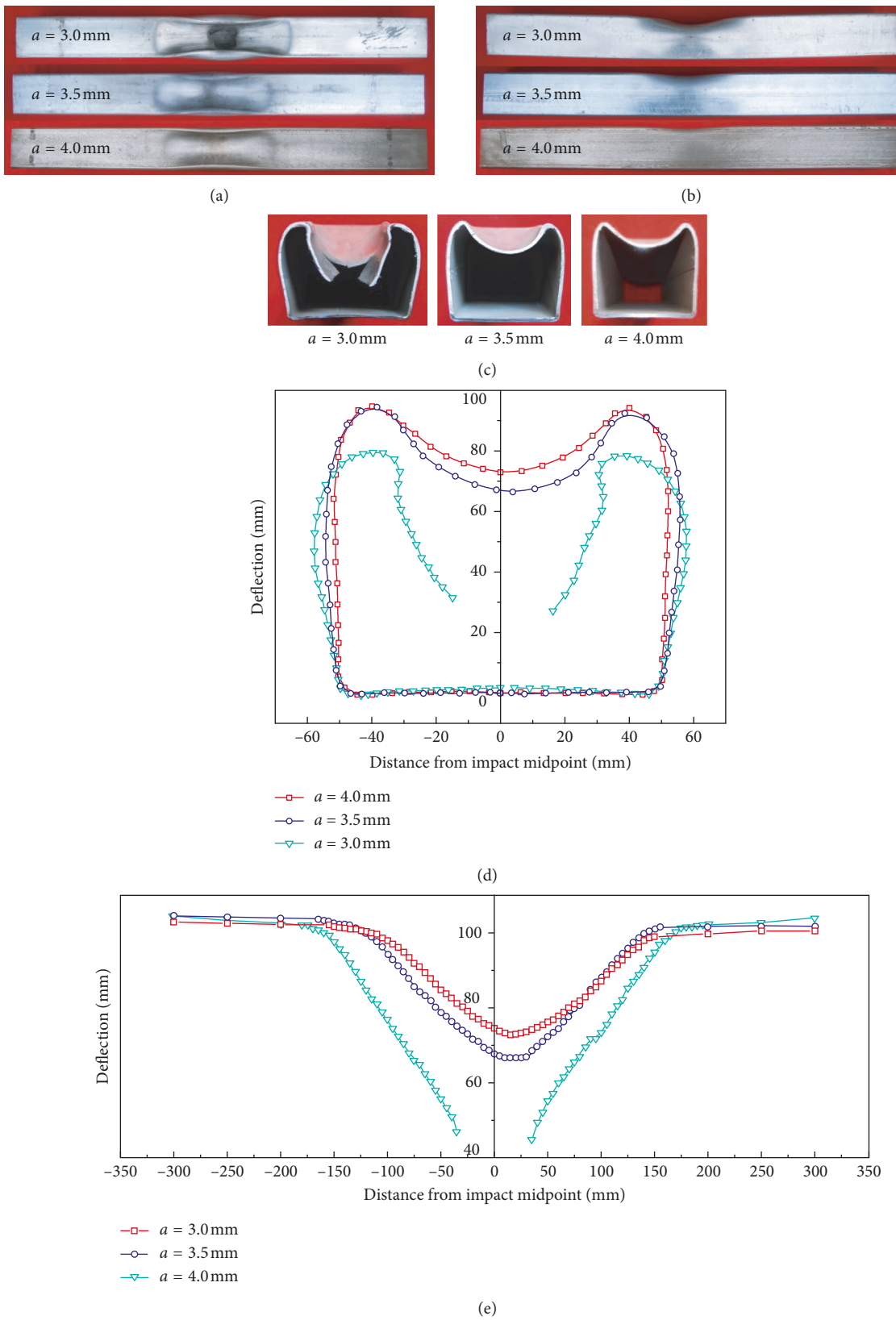

Figure 15: Damage of square tubes with different thicknesses at a stand-off distance of 18 cm. (a) Planform view. (b) Side view. (c) Cross section. (d) Deformation curve on cross section. (e) Deflection in axial direction.

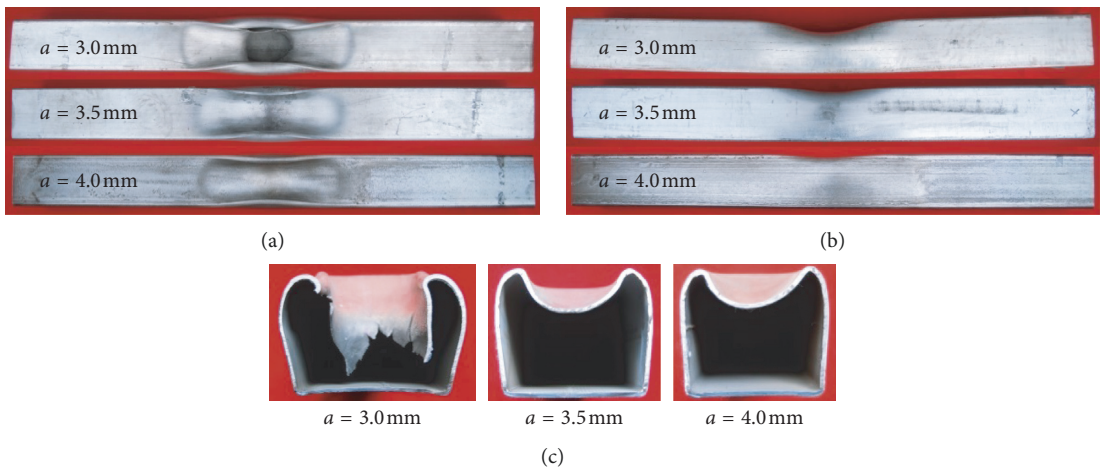

FIGURE 16: Damage of square tubes with different thicknesses at a stand-off distance of 16 cm. (a) Planform view. (b) Side view. (c) Cross section.

become gradually more severe as the wall thickness decreases.

Figure 15 shows that the wall thickness has an important influence on the deformation mode of the square tube subjected to a double explosion. When the stand-off distance is 12 cm and the charge mass is 100 g + 160 g, the deformation mode of the square tube is Mode II for the tubes with thicknesses of 3.5 mm or 4.0 mm and Mode III for the tube with a thickness of 3.0 mm. Although the ultimate rupture strength of the square tube for the different wall thicknesses is equal, the deformation and damage extent of the tube with a thickness of 3.0 mm are the largest compared with those of the tubes with thicknesses of 3.5 mm and 4.0 mm, for a given charge mass and stand-off distance. Besides, when the wall thickness decreases from 4 mm to 3.5 mm, the global deformation value, δ_{global}, increases by 9.1 mm, namely, from 107.8 mm to 116.9 mm, compared with the case where the wall thickness changes from 3.5 mm to 3.0 mm, in which it increases by 24.6 mm, namely, from 116.9 mm to 141.5 mm. From this result, it is obvious that the deformation in the latter case is considerably larger than that in the former one, although the decrease in wall thicknesses is equal in both cases. Figure 15(d) shows the deflection on the cross section of the square tubes for three values of wall thickness. The cross section of the square tube becomes wider as the wall thickness decreases, which, remarkably, weakens the ability of the square tube to resist bending. Figure 15(e) illustrates the axial deformation curve of the square tubes. The deformation of the square tube is still localised in spite of the rupture of the square-tube structure.

In order to quantitatively analyse the damage and dynamic response characteristics of the square tube with different wall thicknesses subjected to explosion loading, the stand-off distance $R = 20$ cm is taken as an example. The gain coefficient v of the depression area V with the wall thickness W is introduced. The gain coefficient v is defined as

$$v = \frac{V_{3.0} - V_{3.5}}{V_{3.5} - V_{4.0}}, \tag{3}$$

where $V_{3.0}$, $V_{3.5}$, and $V_{4.0}$ are the volumes of the depression area when the wall thicknesses are 3, 3.5, and 4.0 mm, respectively.

According to the definition and experimental data in Table 3, when the thickness of a decreases from 4.0 mm to 3.5 mm and from 3.5 mm to 3.0 mm, the volume change of the depression area increases by 6.85 times ($v = 6.85$). It can be seen that the change in wall thickness has a considerable influence on the change in volume of the depression area under the effect of the explosion load.

As can be seen from the above analysis, with the decrease in the wall thickness of a square tube, the corresponding degrees of deformation and damage are increased. Furthermore, when the wall thickness of the tube is reduced for the same interval (4.0 mm to 3.5 mm and 3.5 mm to 3.0 mm), the antiexplosion capability of the tube rapidly decreases. In practical engineering applications, the wall thickness of a square tube should be increased to strengthen the resistance capability of the square-tube structure under a double explosion. Moreover, the construction cost and efficiency of the project should be considered.

4. Conclusions

The main purpose of this study was to investigate the deformation and fracture of steel square tubes under double-explosion loadings. To achieve this purpose, square tubes with different wall thicknesses were subjected to a single explosion (with 160 g of TNT charge) and a double explosion (the first explosion with 100 g of TNT charge and the second explosion with 160 g of TNT charge) with different stand-off distances.

The results obtained from this study are summarised as follows:

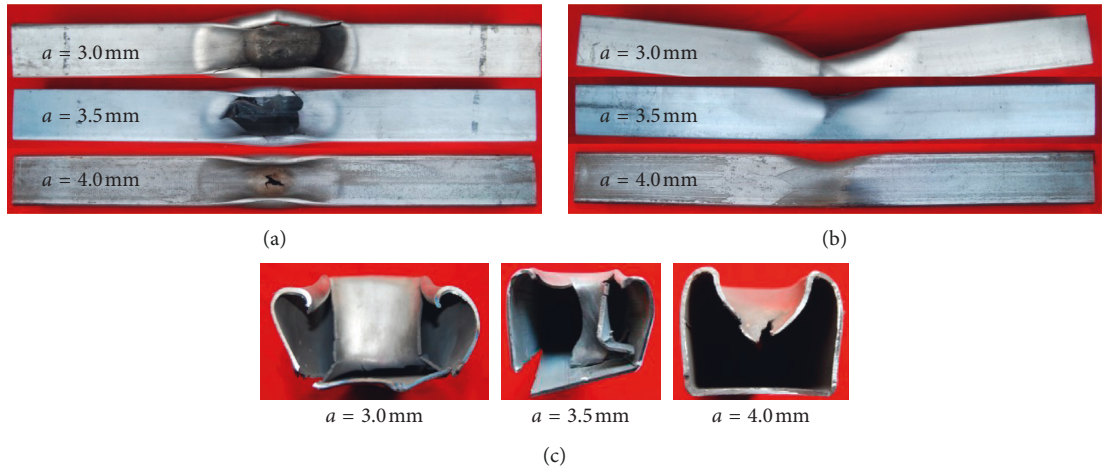

Figure 17: Damage of square tubes with different thicknesses at a stand-off distance of 12 cm. (a) Planform view. (b) Side view. (c) Cross section.

(1) Four major failure modes were recorded during the explosion tests, namely, Mode Ia, Mode Ib, Mode II, and Mode III. Mode Ia denotes local plastic deformation; Mode Ib denotes local plastic deformation with a small global deformation, in which the energy absorbed by the square tube is mainly converted to plastic work. Mode II and Mode III represent different fracture types at the front zone of the square tube with various degrees of deformation, and the energy absorbed by the square tube was mainly converted to plastic work and fracture energy.

(2) As the failure mode of the square tube is transformed from Mode II to Mode III, the fracture pattern changes from the radial H-type crack to axial H-type crack, respectively. The cracks in the radial direction no longer increase owing to the presence of the side corners of the square tube, while the length of the cracks in the side corners of the square tube increases in the axial direction. Mode III presents a completely different crack development path from that of Mode II, and the crack of Mode II is more localised on the front zone.

(3) The failure degrees of square tubes under a double explosion were relatively higher than those of square tubes under a single explosion, namely, the predamaged square tube is more susceptible to damage than an undamaged tube when it undergoes the explosion loading once again. When the stand-off distance or the thickness was small, the difference in failure degree was remarkably obvious.

(4) The experiment indicates that the side corners of the square tube are very vulnerable, and they easily sustain damage owing to the stress concentration and shear effect. This phenomenon is very unfavourable for the stability of square-tube structures in engineering applications.

Future research work will be focused on the numerical simulation of the dynamic responses and damages of square tubes subjected to multiple blast loads.

Data Availability

The data used to support the findings of this study are available from the corresponding author upon request.

Conflicts of Interest

The authors declare that they have no conflicts of interest.

Acknowledgments

This research was supported by the National Natural Science Foundation of China (nos. 51678567 and 11102233) and the China Postdoctoral Science Foundation (nos. 2015M582791 and 2016T90998). The authors would like to gratefully acknowledge this support.

References

[1] S. C. K. Yuen, G. N. Nurick, H. B. Brinckmann, and D. Blakemore, "Response of cylindrical shells to lateral blast load," *International Journal of Protective Structures*, vol. 4, no. 3, pp. 209–230, 2013.

[2] F. Gao, C. Ji, Y. Long, and K. Song, "Dynamic responses and damages of water-filled cylindrical shell subjected to explosion impact laterally," *Latin American Journal of Solids and Structures*, vol. 11, no. 11, pp. 1924–1940, 2014.

[3] K. Song, Y. Long, C. Ji, and F. Gao, "Plastic deformation of metal tubes subjected to lateral blast loads," *Mathematical Problems in Engineering*, vol. 2014, Article ID 250379, 10 pages, 2014.

[4] S. K. Clubley, "Non-linear long duration blast loading of cylindrical shell structures," *Engineering Structures*, vol. 59, pp. 113–126, 2014.

[5] H. C. Kim, D. K. Shin, J. J. Lee et al., "Characteristics of aluminum/CFRP short square hollow section beam under transverse quasi–static loading," *Composites Part B: Engineering*, vol. 51, pp. 345–358, 2014.

[6] A. S. Abedi, N. Hataf, and A. Ghahramani, "Analytical solution of the dynamic response of buried pipelines under blast wave," *International Journal of Rock Mechanics and Mining Sciences*, vol. 88, pp. 301–306, 2016.

[7] J. Wu, C. Ji, Y. Long, K. Song, and Q. Liu, "Dynamic responses and damage of cylindrical shells under the combined effects of fragments and shock waves," *Thin-Walled Structures*, vol. 113, pp. 94–103, 2017.

[8] R. Rajabiehfard, A. Darvizeh, M. Darvizeh, R. Ansari, M. Alitavoli, and H. Sadeghi, "Theoretical and experimental analysis of elastic-plastic cylindrical shells under two types of axial impacts," *Thin-Walled Structures*, vol. 107, pp. 315–326, 2016.

[9] N. Rushton, G. K. Schleyer, A. M. Clayton, and S. Thompson, "Internal explosive loading of steel pipes," *Thin-Walled Structures*, vol. 46, no. 7–9, pp. 870–877, 2008.

[10] R. B. Wegener and J. B. Martin, "Predictions of permanent deformation of impulsively loaded simply supported square tubes steel beams," *International Journal of Mechanical Sciences*, vol. 27, no. 1-2, pp. 55–69, 1985.

[11] M. R. Bambach, "Behaviour and design of aluminium hollow sections subjected to transverse blast loads," *Thin-Walled Structures*, vol. 46, no. 12, pp. 1370–1381, 2008.

[12] M. R. Bambach, "Design of metal hollow section tubular columns subjected to transverse blast loads," *Thin-Walled Structures*, vol. 68, no. 68, pp. 92–105, 2013.

[13] H. H. Jama, M. R. Bambach, G. N. Nurick, R. H. Grzebieta, and X. L. Zhao, "Numerical modelling of square tubular steel beams subjected to transverse blast loads," *Thin-Walled Structures*, vol. 47, no. 12, pp. 1523–1534, 2014.

[14] H. H. Jama, G. N. Nurick, M. R. Bambach, R. H. Grzebieta, and X. L. Zhao, "Steel square hollow sections subjected to transverse blast loads," *Thin-Walled Structures*, vol. 53, pp. 109–122, 2012.

[15] D. Karagiozova, T. X. Yu, G. Lu, and X. Xiang, "Response of a circular metallic hollow beam to an impulsive loading," *Thin-Walled Structures*, vol. 80, pp. 80–90, 2014.

[16] D. Karagiozova, T. X. Yu, and G. Lu, "Transverse blast loading of hollow beams with square cross-sections," *Thin-Walled Structures*, vol. 62, pp. 169–178, 2013.

[17] N. Jones, "The credibility of predictions for structural designs subjected to large dynamic loadings causing inelastic behavior," *International Journal of Impact Engineering*, vol. 53, pp. 106–114, 2013.

[18] Y. Zhang, Q. Fang, L. Chen et al., "Blast-resistant properties of reinforced concrete and steel beams subjected to multiple blast loads," *Acta Armamentarii*, vol. 30, pp. 182–187, 2009, in Chinese.

[19] M. Kumar, M. D. Goel, V. A. Matsagar, and K. S. Rao, "Response of semi–buried structures subjected to multiple blast loading considering soil-structure interaction," *Indian Geotechnical Journal*, vol. 45, no. 3, pp. 243–253, 2015.

[20] T. F. Henchie, S. C. K. Yuen, G. N. Nurick, N. Ranwaha, and V. H. Balden, "The response of circular plates to repeated uniform blast loads: an experimental and numerical study," *International Journal of Impact Engineering*, vol. 74, pp. 36–45, 2014.

[21] S. C. K. Yuen, G. Nurick, N. Ranwaha, and T. Henchie, "The response of circular plates to repeated uniform blast loads," *Key Engineering Materials*, vol. 535-536, pp. 44–47, 2013.

[22] Y. Zhou, C. Ji, Y. Long, Y. Yu, Y. Li, and T. Wang, "Experimental studies on the deformation and damage of steel cylindrical shells subjected to double-explosion loadings," *Thin-Walled Structures*, vol. 127, pp. 469–482, 2018.

[23] S. B. Menkes and H. Opat, "Broken beams," *Experimental Mechanics*, vol. 13, no. 11, pp. 480–486, 1973.

[24] G. F. Kinney and K. J. Graham, *Explosive Shocks in Air*, Springer, New York, NY, USA, 1985.

[25] R. K. Wharton, S. A. Formby, and R. Merrifield, "Air–blast TNT equivalence for a range of commercial blasting explosives," *Journal of Hazardous Materials*, vol. 79, no. 1-2, pp. 31–39, 2000.